Enhanced Piezoelectric Response of Layered In_2Se_3/MoS_2 Nanosheet-Based van der Waals Heterostructures

Shuoguo Yuan[1], Weng Fu Io[1], Jianfeng Mao[1], Yancong Chen[2], Xin Luo[2], Jianhua Hao[1]**

[1]Department of Applied Physics, The Hong Kong Polytechnic University, Kowloon, Hong Kong, P. R. China

[2]State Key Laboratory of Optoelectronic Materials and Technologies, Centre for Physical Mechanics and Biophysics, School of Physics, Sun Yat-sen University, Guangzhou 510275, P. R. China

Corresponding Author

* jh.hao@polyu.edu.hk. * luox77@mail.sysu.edu.cn.

ABSTRACT: Two-dimensional (2D) piezoelectricity has been extensively addressed in recent years, which leads to great potential applications in advanced smart devices. However, the vertical piezoelectric response of numerous 2D layered materials is theoretically absent when applying electric field or strain perpendicular to its surface because of the inversion symmetry. Recently, vertical piezoelectric properties of In_2Se_3, which exhibits low piezoelectric response,

were reported. Therefore, enhancing the piezoelectric performance in 2D layered materials is still challenging. Here, we report a remarkable out-of-plane piezoelectric performance in the In_2Se_3/MoS_2 van der Waals (vdW) heterostructure. Such a vdW heterostructure shows a high positive value of piezoelectric coefficient d_{33}. By combining the experimental studies and density functional theory calculations, the excellent piezoelectric properties result from the type II band alignment, which causes a larger interfacial dipole moment. Moreover, the high-precision piezoelectric actuators in 2D atomic scale are demonstrated. By changing the driven voltage, the deformation of the upper surface of piezoelectric actuators linearly modulated. Our study opens the door to design next-generation nanoelectronics and multifunctional coupling atomic-scale devices.

KEYWORDS

two-dimensional material, van der Waals heterostructure, piezoelectricity, actuator, In_2Se_3

1. INTRODUCTION

Conventional piezoelectric materials based on $Pb(Zr,Ti)O_3$ have been used in various applications, for instance, transducers, sensors, actuators and energy harvesting, etc.[1-6] Recently, piezoelectricity in two-dimensional (2D) layered materials has attracted enormous interest owing to promising unique applications in nanoscale electromechanical systems, ultrasensitive sensors, high-precision actuators, piezotronics, piezo-phototronics and energy conversion.[7-10] The in-plane piezoelectricity has been experimentally existing in monolayer MoS_2,[8-11] WSe_2,[12,13] g-C_3N_4,[14] SnS,[15] and Se,[16] which may not be suitable for wide applications in the vertical structural nano-electromechnical systems. Currently, piezoelectricity in 2D material family has largely been predicted by theoretical calculations,[17-19] but still few experimental observations from others so far. Recent studies have reported that out-of-plane piezoelectricity existed in MoSSe and α-In_2Se_3, which exhibits low piezoelectric response.[20-22] Therefore, enhancing the piezoelectric performance in 2D layered materials is still challenging. The van der Waals (vdW) heterostructure engineering can be employed to generate the novel physical phenomena and performance, providing an important approach to improve various physical properties of 2D layered materials.[23-26] To our best knowledge, there is still no experimental study on the enhanced out-of-plane intrinsic piezoelectric performance via vdW heterostructure engineering.

Here, we report that the remarkable out-of-plane piezoelectric response is achieved in 2D vdW heterostructure system with In_2Se_3/MoS_2, which is different from in-plane piezoelectricity MoS_2 restricted by edge effect and odd-even layers. In addition, physical mechanism of piezoelectric properties of vdW heterostructure is studied. Moreover, a high-precision piezoelectric actuator in 2D atomic scale is demonstrated, which will result in unexpected applications in nanoelectronics and atomic-scale multifunctional coupling devices.

2. EXPERIMENTAL SECTION

Preparation and characterization of samples: The In_2Se_3 and MoS_2 nanosheets were prepared using mechanical exfoliation, and the MoS_2 and WS_2 were prepared by chemical vapor deposition. The MoO_3 or WO_3 precursor powder and the substrate were placed at the downstream and S powder was placed in another quartz boat in the upstream of quartz tube, and then these powders were heated and held at their respective temperature. After chemical growth process, the furnaces were cooled down to room temperature. The In_2Se_3/MoS_2 and In_2Se_3/WS_2 heterostructures were fabricated by dry transfer method (Scheme S1). The Raman spectra, PL mapping and spectra of the samples were measured by Raman spectroscopy (Witec Confocal Raman system alpha 300 R). Microstructures and chemical compositions were examined by transmission electron microscope (JEOL JEM 2100F) equipped with EDX. The composition of samples was obtained by using X-ray photoelectron spectroscopy (XPS, Thermol Escalab 250Xi, Al Kα radiation). The UPS measurement was performed with regular photon energy of 21.2 eV (Helium I). A femtosecond laser with the wavelength of 798 nm was utilized to characterize the second-harmonic signals of samples. The PFM images were performanced on a commercial atomic force microscope (Asylum Research MFP-3D), a tip was driven with an ac voltage (V_{ac} = 0.2～4 V) under the tip-sample contact resonant frequency (～300 kHz).

DFT calculations: The DFT calculations were performed with the VASP code using the projector-augmented plane wave (PAW) approach and a kinetic energy cut-off of 500 eV. The generalized gradient approximation (GGA) with Perdew-Burke-Ernzerhof (PBE) exchange-correlation functional was employed to perform all calculations and Grimme's D3 correction was used to consider the vdW interactions.[27] The optimized lattice constant of single layer In_2Se_3 and MoS_2 is 4.10 Å and 3.18 Å, respectively. To have a smaller lattice mismatch, the In_2Se_3/MoS_2 heterostructure contains a 2×2×1 supercell of In_2Se_3

and a 19° rotated MoS_2 supercell, with a total number of 41 atoms. A vacuum thickness of 20 Å is added in the slab to minimize the interaction between adjacent image cells. Geometry optimization was performed with a force convergence criterion of 0.01 eV/Å. Monkhorst Pack k-grid sampling of 5×5×1 was used for geometry optimization in the heterostructures.

3. RESULTS AND DISCUSSION

3.1. Structural Characterizations of α-In_2Se_3. Each α-In_2Se_3 quintuple layer contains the atomic lattices stacked in the sequence of Se-In-Se-In-Se. **Figure 1**a shows the atomic structure of the α-In_2Se_3. The middle position of the Se atom shifted off-center breaks the centrosymmetry, leading to out-of-plane piezoelectricity. In order to evaluate the piezoelectric performance in α-In_2Se_3, we prepared the α-In_2Se_3 nanosheets which were exfoliated from bulk materials. The optical microscopical and corresponding atomic force microscope images of exfoliated In_2Se_3 nanosheets are shown in Figure S1, Supporting Information. To characterize the structure of the In_2Se_3, Raman spectroscopy is widely used by the characteristic Raman vibration modes. **Figure 1b** reveals thickness dependance of Raman spectra of In_2Se_3. Typically, the α phase In_2Se_3 exhibits two characteristic Raman peaks at 180 cm^{-1} and 195 cm^{-1}, corresponding to A(LO) mode. In addition, it is noted that α phase In_2Se_3 also includes two additional Raman peaks below 150 cm^{-1} which are near 90 cm^{-1} and 104 cm^{-1}, relating to E mode and A(LO+TO) mode (Figure S1, Supporting Information), which is in agreement with earlier work.[21] To characterize the elemental composition and chemical environment in the In_2Se_3, X-ray photoelectron spectroscopy (XPS) spectra of In_2Se_3 are shown in **Figure 1c**. The XPS spectra show that the signatures of In and Se elements corresponds to In and Se 3d states, implying excellent purity of the samples. The atomic ratio of In/Se is further confirmed by elemental mapping and energy

dispersive spectroscopy (**Figure 1d,e**; Figure S1, Supporting Information), which is consistent with XPS result. The structural characterization of In_2Se_3 was measured from transmission electron microscopy (TEM). **Figure 1f** shows TEM image of In_2Se_3 nanosheets and the inset presents the selected area electron diffraction (SAED) pattern of In_2Se_3. The symmetric diffraction pattern validates α phase In_2Se_3 with hexagonal structure.

3.2. Piezoelectric Properties of α-In_2Se_3. Piezoresponse force microscope (PFM) is usually used to measure the converse piezoelectric response which represents out-of-plane deformation by applying a vertical electric field. Piezoelectric materials are deformed under applied electrical field, which will result in the amplitude change generated in PFM imaging. The piezoelectric coefficient d_{33} is to quantify the piezoelectric properties of samples. To obtain a quantitative estimation of the true piezoelectric response and minimize the contribution from nonelectromechanical effects, a background subtraction method is employed. In addition, the samples fabricated on non-piezoelectric substrates (SiO_2/Si) could eliminate background contribution of the measured In_2Se_3 signal. Here, we used PFM to measure the out-of-plane piezoelectricity of In_2Se_3 onto SiO_2/Si substrates. As shown in **Figure 2a-e**, we observe a clear piezoelectric contrast in the In_2Se_3. The obvious contrast can not result from the surface topographic or electromechanical artefacts, because the substrate does not give visible contrast with the coincident measurement condition. The PFM amplitude images reveal strong piezoelectric responses, demonstrating the existence of out-of-plane piezoelectricity in In_2Se_3 due to the non-centrosymmetric structure. The non-centrosymmetric structure of In_2Se_3 is further confirmed by second-harmonic generation (Figure S2, Supporting Information). In addition, the vertical PFM amplitude increases with increasing voltages. The relationship between vertical amplitude and applied drive voltage for In_2Se_3 is plotted (**Figure 2f**), and the piezoelectric

coefficient d_{33} can be directly obtained from the fitting slope. The out-of-plane piezoelectric coefficient d_{33} of 80 nm In_2Se_3 onto SiO_2/Si substrate is estimated to be around 7.6 pm/V, which is similar to the reported value.[22] In addition, the piezoelectric coefficient d_{33} decreases with decreasing the layer-number (Figure S2, Supporting Information), and the decrease of piezoelectric response with reducing number of layers may be due to the substrate constraint. Typically, the out-of-plane piezoelectric response of most-common 2D compound materials MoS_2 is theoretically absent due to its inversion symmetry. For comparison, we carried out the piezoelectric response of the chemical vapor deposition (CVD) grown monolayer MoS_2 by PFM. We do not observe the obvious piezoresponse signal because of its symmetry structure (Figure S3, Supporting Information). In addition, the monolayer MoS_2 nanosheet was prepared by mechanical exfoliation and measured by the same PFM measurement. Similarly, no obvious vertical piezoelectric signal is obtained, also confirming the accuracy of the vertical piezoelectric measurements (Figure S4, Supporting Information).

3.3. Piezoelectric Properties of In_2Se_3/MoS_2 vdW Heterostructure. To estimate the piezoelectric properties of In_2Se_3/MoS_2 vdW heterostructure, we prepared the In_2Se_3/MoS_2 (Raman and PL spectra of In_2Se_3/MoS_2 are shown in Figure S5, Supporting Information) and measured its piezoelectric properties. As shown in **Figure 3a-h**, the obvious piezoelectric contrast can be seen in the In_2Se_3/MoS_2 heterostructure, and the piezoelectric response signal increases with varying the drive voltage (Figure S6, Supporting Information). The piezoelectric coefficient d_{33} of In_2Se_3/MoS_2 heterostructure is estimated to be approximately 17.5 pm/V. In addition, the thickness dependence of the piezoelectric coefficient d_{33} of In_2Se_3/MoS_2 is shown in **Figure 3I**. The piezoelectric coefficient d_{33} shows the increase trend with increasing the layer

number. When the nanosheet thickness exceeds 40 nm, the related piezoelectric coefficient sequentially increases to a relative saturated value.

3.4. Physical Mechanism of Piezoelectric Performance. The enhanced piezoelectric properties of In_2Se_3/MoS_2 vdW heterostructure could be achieved, which is attributed to large band offset.[28] The piezoelectric effect can be controlled by the interfacial polarization charges, which is relevant to the band alignment with offset. The atomic structure of In_2Se_3/MoS_2 is shown in **Figure 4a**. The large band offset of the conduction band minimum (CBM) and the valence band maximum (VBM) between In_2Se_3 and MoS_2 atomic layers leads to large electric polarization, as shown in Figure 4b. To understand the energy band between In_2Se_3 and MoS_2, the ultraviolet photoelectron spectroscopy (UPS) spectra were carried out, as shown in **Figure 4c-f**. By linearly extrapolating the secondary electron cut off edge of the UPS spectra to the baseline, the energy of the cut off edge is observed to be 16.9 eV. The work function (ϕ) of the In_2Se_3 is calculated to be 4.3 eV, according to the equation $\phi = h\nu - E_{cutoff}$ with the incident photon energy $h\nu$=21.2 eV. In addition, the VBM is performed by linearly extrapolating the onset edge of the UPS spectrum to the baseline, the difference between the Fermi energy and the valence band is found to be 1.15 eV. Similarly, the work function (ϕ) of the MoS_2 is calculated to be 3.9 eV and the valence band maximum is determined to be 1.25 eV. According the bandgap of In_2Se_3 and MoS_2, a large band offset of In_2Se_3 and MoS_2 is found to be 0.8 eV (**Figure 4b**). The large band offset leads to a strong polarization which results in the remarkable piezoelectricity of the In_2Se_3/MoS_2 heterostructure.

It is noted that the above work function and VBM information are measured in isolated In_2Se_3 (or transition metal dichalcogenides), the combination of In_2Se_3 and individual MoS_2 material may cause different band alignment due to the charge transfer at the interface of the In_2Se_3/MoS_2

heterostructure.[29-32] To figure out the influence of the interfacial charge transfer and the possible screening effect on the band alignment, we calculate the band structure and differential charge density of the In_2Se_3/MoS_2 heterostructure. The calculated bandgap of the In_2Se_3 and MoS_2 is respectively 0.83 and 1.83 eV, slightly smaller than the experimental measured optical bandgap of 1.38 eV and 1.86 eV respectively. The PBE calculated bandgap usually underestimates the actual bandgap due to the complicated self-interaction error arising in the occupied states in standard density functional theory (DFT). A more accurate bandgap could be obtained with the many-electron quasi-partical GW calculations. However, the computation is prohibitive in our supercell heterostructure system. From the calculated band structure, it is found that when the polarization is pointing towards the MoS_2 layer, the heterostructure's band structure forms the type I band alignment (**Figure 5a**), that is, the CBM and VBM of In_2Se_3 is completely within the bandgap of MoS_2. On the other hand, the heterostructure has the type II band alignment when the polarization of In_2Se_3 is point upward away from the MoS_2 (**Figure 5b**). The CBM is contributed by the In_2Se_3 layer and the VBM is contributed by the MoS_2 layer in the type II band alignment, which will enhance the total polarization due to the additional interfacial dipole moment as shown in **Figure 5d**, the large charge transfers in the type II band alignment causes a larger interfacial dipole moment. By comparing the calculated total energy, we notice that the structure where the polarization is pointing upward is more stable than that has the polarization downward, with an energy gain of 70 meV. Based on the large energy gain, it is expected that type II band alignment could be formed in the experimental heterostructure. Compared to single In_2Se_3, the type II band alignment is more helpful for the interfacial charge transfer of vdW heterostructure. The DFT calculation is also consistent with the experimental band alignment obtained from the UPS measurement if the vacuum level is used as a reference level.

In addition to the In_2Se_3/MoS_2 vdW heterostructure, we also applied the heterostructure engineering to other 2D materials such as WS_2 to determine the piezoelectric properties. Similarly, a smaller piezoelectric performance in the In_2Se_3/WS_2 vdW heterostructure is acquired due to smaller band offset (Figure S7, S8, and S9, Supporting Information), which exhibits its potential for establishing a wide range of 2D material heterostructures with multifunctionalities.

The calculated piezoelectric coefficients of the In_2Se_3/MoS_2 with the polarization pointing towards MoS_2 (P_1) and away from MoS_2 (P_2) are shown in Table S2, Supporting Information. Compared with the monolayer In_2Se_3, the in-plane piezoelectric coefficient is of similar value, but the out-of-plane piezoelectric coefficient is significantly enhanced in the In_2Se_3/MoS_2 heterostructure. A similar trend is also found in the In_2Se_3/WS_2, although the exact value is smaller.

3.5. Piezoelectric Actuator Applications. The most important application of the piezoelectric material is in an actuator where the strain is induced by an electric field. The development of high-precision actuators will facilitate the precise location down to nanometer scale, which have been used for wide applications, such as scanning probe microscopy.[33] To reveal the experimental vertical piezoelectricity and estimate the deformation under applied dc voltage, for simplicity, we have designed the subatomic deformation actuators based on the measured piezoelectric properties of In_2Se_3. We estimate the thickness dependent piezoresponse loops of In_2Se_3 shown in Figure S10, Supporting Information. The effective out-of-plane piezoelectric coefficient d_{33} of In_2Se_3 is estimated to be around 90.6 pm/V. To compare with the experimental observed piezoelectricity and deformation of In_2Se_3, we employed a 3D finite element (FE) model with COMSOL Multiphysics. The simulation model consists of a round In_2Se_3 sample with thickness of 11 nm (～11 layers) and diameter of 30 nm. A direct current voltage was

applied on the upper surface of the sample and the lower surface was electrical grounding (U=0) and fixed constraint in z direction (displacement u=0). For In_2Se_3 material, the used elastic matrix C_{ij} was set to the unstrained elastic constants as list in Table S3, Supporting Information. Deformation of 11 nm thick In_2Se_3 sample is shown in **Figure 6a** with −8 V voltage applied. By changing the driven voltage from −8 V to −1 V, the deformation of the upper surface along the *x* axis linearly decreased from +0.008 nm to −0.001 nm (**Figure 6b**). **Figure 6c** shows the simulation results of a strained In_2Se_3 mapping with different voltages applied to its upper surface. When we decreased the thickness of In_2Se_3 sample from 11 nm to nearly monolayer (1 nm), vertical deformation changed linearly under different voltage (**Figure 6d**).

Currently, transition metal dichalcogenides are intrinsically in-plane piezoelectricity, which results from the lack of inversion symmetry along in-plane direction. For example, in-plane piezoelectricity only exists in odd-layer and zigzag-edge for typical 2D materials MoS_2, and the piezoelectric response significantly reduces and disappears with increasing layer numbers. Meanwhile, the out-of-plane piezoelectricity in the MoS_2 theoretically yields no piezoelectric response thanks to its centrosymmetric structure. Moreover, several reported 2D piezoelectric materials are commonly limited to the in-plane direction of odd-number ultrathin layers and the piezoelectric response significantly reduced and disappears with increasing layer numbers, which largely restricts their broad applications. Very recently, the polar symmetry alteration at the interface was found to induce the out-of-plane piezoelectricity, which was experimentally studied in metal-semiconductor heterostructure.[5] The present work demonstrates that the piezoelectric coefficient d_{33} of combined In_2Se_3/MoS_2 vdW heterostructure system is larger than the individual In_2Se_3 and MoS_2.[22] Meanwhile, the piezoelectric coefficient d_{33} is also larger than that of the widely used piezoelectric thin films and ultrathin piezoelectric materials (Table S1,

Supporting Information).[34,35] It is noted that the reported d_{33} is the high positive piezoelectric coefficient value in the 2D layered piezoelectric materials. Moreover, typical 2D materials are flexible and easy to be integrated with conventional integrated circuits or microelectromechanical systems. As a result, designing and constructing the vertical piezoelectricity in the novel 2D heterostructure will explore the rich physics and unique possibilities of the 2D piezoelectric materials, which will expand and create the unprecedented applications of 2D piezoelectric materials.

4. CONCLUSIONS

In summary, we have demonstrated superior out-of-plane piezoelectric coefficient d_{33} of approximate 17.5 pm/V for In_2Se_3/MoS_2 vdW heterostructure. The enhanced piezoelectric properties of In_2Se_3/MoS_2 are ascribed to a larger interfacial dipole moment result from the type II band alignment. In addition, the vdW heterostructure can be extended to other 2D materials like WS_2. Moreover, the atomical deformation actuator based on out-of-plane piezoelectricity is demonstrated. As a result, current study opens an alternative approach in designing novel multifunctional coupling atomic-scale nanoelectronics devices.

ASSOCIATED CONTENT

Supporting Information

The Supporting Information is available free of charge.

Optical microscope, atomic force microscope, Raman spectra, PFM amplitude image, thickness dependent of piezoelectric coefficient, CVD grown monolayer MoS_2 and WS_2, UPS spectra of vdW heterostructure (PDF)

AUTHOR INFORMATION

Present Addresses

Shuoguo Yuan, Weng Fu Io, Jianfeng Mao, Jianhua Hao

Department of Applied Physics, The Hong Kong Polytechnic University, Kowloon, Hong Kong, P. R. China

Yancong Chen, Xin Luo

State Key Laboratory of Optoelectronic Materials and Technologies, Centre for Physical Mechanics and Biophysics, School of Physics, Sun Yat-sen University, Guangzhou 510275, P. R. China

Notes

The authors declare no competing financial interest.

ACKNOWLEDGMENT

This work was supported by the grants from Research Grants Council of Hong Kong (GRF No. PolyU 153025/19P) and PolyU Grant (UABC). X.L. also thanks support from the NSFC (No. 11804286 and 11832019) and the Fundamental Research Funds for the Central Universities (No. 19lgpy263). The calculations were supported by the Special Program for Applied Research on Super Computation of the NSFC Guangdong Joint Fund (the second phase).

REFERENCES

(1) Qiu, C.; Wang, B.; Zhang, N.; Zhang, S.; Liu, J.; Walker, D.; Wang, Y.; Tian, H.; Shrout, T. R.; Xu, Z.; Chen, L.; Li, F. Transparent ferroelectric crystals with ultrahigh piezoelectricity. *Nature* **2020**, *577*, 350-354.

(2) Liu, H.; Wu, H.; Ong, K. P.; Yang, T; Yang, P.; Das, P. K.; Chi, X.; Zhang, Y.; Diao, C., Wong, W. K. A.; Chew, E. P.; Chen, Y. F.; Tan, C. K. I.; Rusydi, A.; Breese, M. B. H.; Singh, D. J.; Chen, L.; Pennycook, S. J.; Yao, K. Giant piezoelectricity in oxide thin films with nanopillar structure. *Science* **2020**, *369*, 292-297.

(3) Liao, W.; Zhao, D.; Tang, Y.; Zhang, Y.; Li, P.; Shi, P.; Chen, X.; You, Y.; Xiong, R. A molecular perovskite solid solution with piezoelectricity stronger than lead zirconate titanate. *Science* **2019**, *363*, 1206-1210.

(4) Yuan, S.; Luo, X.; Chan, H. L.; Xiao, C.; Dai, Y.; Xie, M.; Hao, J. Room-temperature ferroelectricity in $MoTe_2$ down to the atomic monolayer limit. *Nat. Commun.* **2019**, *10*, 1775.

(5) Yang, M.; Luo, Z.; Mi, Z.; Zhao, J.; Pei, E S.; Alexe, M. Piezoelectric and pyroelectric effects induced by interface polar symmetry. *Nature* **2020**, *584*, 377-381.

(6) Ghasemian, M. B.; Zavabeti, A.; Abbasi, R.; Kumar, P. V.; Syed, N.; Yao, Y.; Tang, J.; Wang, Y.; Elbourne, A.; Han, J.; Mousavi, M.; Daeneke, T.; Kalantar-Zadeh, K. Ultra-thin lead oxide piezoelectric layers for reduced environmental contamination using a liquid metal-based process. *J. Mater. Chem. A* **2020**, *8*, 19434.

(7) Wu, W. & Wang, Z. L. Piezotronics and piezo-phototronics for adaptive electronics and optoelectronics. *Nat. Rev. Mater.* **2016**, *1*, 16031.

(8) Wu, W.; Wang, L.; Li, Y.; Zhang, F.; Lin, L.; Niu, S.; Chenet, D.; Zhang, X.; Hao, Y.; Heinz, T. F.; Hone, J.; Wang, Z. L. Piezoelectricity of single-atomic-layer MoS_2 for energy conversion and piezotronics. *Nature* **2014**, *514*, 470-474.

(9) Zhu, H.; Wang, Y.; Xiao, J.; Liu, M.; Xiong, S.; Wong, Z.; Ye, Z.; Ye, Y.; Yin, X.; Zhang, X. Observation of piezoelectricity in free-standing monolayer MoS_2. *Nat. Nanotechnol.* **2015**, *10*, 151-155.

(10) Hinchet, R.; Khan, U.; Falconi, C.; Kim, S. Piezoelectric properties in two-dimensional materials: simulations and experiments. *Mater. Today* **2018**, *21*, 611-630.

(11) Qi, J.; Lan, Y.; Stieg, A. Z.; Chen, J.; Zhong, Y.; Li, L.; Chen, C.; Zhang, Y., Wang, K. L. Piezoelectric effect in chemical vapour deposition-grown atomic-monolayer triangular molybdenum disulfide piezotronics. *Nat. Commun.* **2015**, *6*, 7430.

(12) Lee, J.; Park, J.; Cho, E. B.; Kim, T. Y.; Han, S. A.; Kim, T.; Liu, Y.; Kim, S. K.; Roh, C. J.; Yoon, H.; Ryu, H.; Seung, W.; Lee, J. S.; Lee, J.; Kim, S. Reliable piezoelectricity in bilayer WSe_2 for piezoelectric nanogenerators. *Adv. Mater.* **2017**, *29*, 1606667.

(13) Esfahani, E. N.; Li, T.; Huang, B.; Xu, X.; Li, J. Piezoelectricity of atomically thin WSe_2 via laterally excited scanning probe microscopy. *Nano Energy* **2018**, *52*, 117-122.

(14) Zelisko, M.; Hanlumyuang, Y.; Yang, S.; Liu, Y.; Lei, C.; Li, J.; Ajayan, P. M.; Sharma, P. Anomalous piezoelectricity in two-dimensional graphene nitride nanosheets. *Nat. Commun.* **2014**, *5*, 4284.

(15) Khan, H.; Mahmood, N.; Zavabeti, A.; Elbourne, A.; Rahman, M. A.; Zhang, B. Y.; Krishnamurthi, V.; Atkin, P.; Ghasemian, M. B.; Yang, J.; Zheng, G.; Ravindran, A. R.; Walia, S.; Wang, L.; Russo, S. P.; Daeneke, T.; Li, Y.; Kalantar-Zadeh, K. Liquid metal-based synthesis of high performance monolayer SnS piezoelectric nanogenerators. *Nat. Commun.* **2020**, *11*, 3449.

(16) Wu, M.; Wang, Y.; Gao, S.; Wang, R.; Ma, C.; Tang, Z.; Bao, N.; Wu, W.; Fan, F.; Wu, W. Solution-synthesized chiral piezoelectric selenium nanowires for wearable self-powered human-integrated monitoring. *Nano Energy* **2019**, *56*, 693-699.

(17) Ding, W.; Zhu, J.; Wang, Z.; Gao, Y.; Xiao, D.; Gu, Y.; Zhang, Z.; Zhu, W. Prediction of intrinsic two-dimensional ferroelectrics in In_2Se_3 and other III_2-VI_3 van der Waals materials. *Nat. Commun.* **2017**, *8*, 14956.

(18) Blonsky, M. N.; Zhuang, H. L.; Singh, A. K.; Hennig, R. G. *Ab Initio* prediction of piezoelectricity in two-dimensional materials. *ACS Nano* **2015**, *9*, 9885-9891.

(19) Michel, K. H.; Çakır, D.; Sevik, C.; Peeters, F. M. Piezoelectricity in two-dimensional materials: comparative study between lattice dynamics and ab initio calculations. *Phys. Rev. B* **2017**, *95*, 125415.

(20) Lu, A.; Zhu, H.; Xiao, J.; Chuu, C.; Han, Y.; Chiu, M.; Cheng, C.; Yang, C.; Wei, K.; Yang, Y.; Wang, Y.; Dimosthenis, S.; Nordlund, D.; Yang, P.; Muller, D. A.; Chou, M.; Zhang, X.; Li, L. Janus monolayers of transition metal dichalcogenides. *Nat. Nanotechnol.* **2017**, *12*, 744-749.

(21) Zhou, Y.; Wu, D.; Zhu, Y.; Cho, Y.; He, Q.; Yang, X.; Herrera, K.; Chu, Z.; Han, Y.; Downer, M. C.; Peng, H.; Lai, K. Out-of-plane piezoelectricity and ferroelectricity in layered α-In_2Se_3 nanoflakes. *Nano Lett.* **2017**, *17*, 5508-5513.

(22) Xue, F.; Zhang, J.; Hu, W.; Hsu, W.; Han, A.; Leung, S.; Huang, J.; Wan, Y.; Liu, S.; Zhang, J.; He, J.; Chang, W.; Wang, Z. L.; Zhang, X.; Li, L. Multidirection piezoelectricity in mono- and multilayered hexagonal α-In_2Se_3. *ACS Nano* **2018**, *12*, 4976-4983.

(23) Novoselov, K. S.; Mishchenko, A.; Carvalho, A.; Castro Neto, A. H. 2D materials and van der Waals heterostructures. *Science* **2016**, *353*, aac9439.

(24) Liu, Y.; Weiss, N. O.; Duan, X.; Cheng, H.; Huang, Y.; Duan, X. Van der Waals integration before and beyond two-dimensional materials. *Nature* **2019**, *567*, 323-333.

(25) Tran, K.; Moody, G.; Wu, F.; Lu, X.; Choi, J.; Kim, K.; Rai, A.; Sanchez, D. A.; Quan, J.; Singh, A.; Embley, J.; Zepeda, A.; Campbell, M.; Autry, T.; Taniguchi, T.; Watanabe, K.; Lu, N.; Banerjee, S. K.; Silverman, K. L.; Kim, S., Tutuc, E.; Yang, L.; MacDonald, A. H.; Li, X. Evidence for moiré excitons in van der Waals heterostructures. *Nature* **2019**, *567*, 71-75.

(26) Li, J.; Yang, X.; Liu, Y.; Huang, B.; Wu, R.; Zhang, Z.; Zhao, B.; Ma, H.; Dang, W.; Wei, Z.; Wang, K.; Lin, Z.; Yan, X.; Sun, M.; Li, B.; Pan X.; Luo, J.; Zhang, G.; Liu, Y.; Huang, Y.; Duan, X.; Duan, X. General synthesis of two-dimensional van der Waals heterostructure arrays. *Nature* **2020**, *579*, 368-374.

(27) Grimme, S.; Antony, J.; Ehrlich, S.; Krieg, H. A consistent and accurate ab initio parametrization of density functional dispersion correction (DFT-D) for the 94 elements H-Pu. *J. Chem. Phys.* **2010**, *132*, 154104.

(28) Yu, S.; Rice, Q.; Tabibi, B.; Li, Q.; Seo, F. J. Piezoelectricity in WSe_2/MoS_2 heterostructure atomic layers. *Nanoscale* **2018**, *10*, 12472-12479.

(29) Zheng, W.; Zheng, B.; Yan, C.; Liu, Y.; Sun, X.; Qi, Z.; Yang, T.; Jiang, Y.; Huang, W.; Fan, P.; Jiang, F.; Ji, W.; Wang, X.; Pan, A. Direct vapor growth of 2D vertical heterostructures with tunable band alignments and interfacial charge transfer behaviors. *Adv. Sci.* **2019**, *6*, 1802204.

(30) Mohanta, M. K.; Rawat, A.; Dimple; Jena, N.; Ahammed R.; De Sarkar, A. Superhigh out-of-plane piezoelectricity, low thermal conductivity and photocatalytic abilities in ultrathin 2D van der Waals heterostructures of boron monophosphide and gallium nitride. *Nanoscale* **2019**, *11*, 21880.

(31) Mohanta, M. K.; Rawat, A.; Jena, N.; Dimple; Ahammed R.; De Sarkar, A. Interfacing boron monophosphide with molybdenum disulfide for an ultrahigh performance in

thermoelectrics, two-dimensional excitonic solar cells, and nanopiezotronics. *ACS Appl. Mater. Interfaces* **2020**, *12*, 3114-3126.

(32) Huang, L.; Li,Y.; Wei, Z.; Li, J. Strain induced piezoelectric effect in black phosphorus and MoS_2 van der Waals heterostructure. *Sci. Rep.* **2015**, *5*, 16448.

(33) Christman, J. A.; Jr., R. R. W.; Kingon, A. I.; Nemanich, R. J. Piezoelectric measurements with atomic force microscopy. *Appl. Phys. Lett.* **1998**, *73*, 3851.

(34) Syed, N.; Zavabeti, A.; Ou, J. Z.; Mohiuddin, M.; Pillai, N.; Carey, B. J.; Zhang, B. Y.; Datta, R. S.; Jannat, A.; Haque, F.; Messalea, K. A.; Xu, C.; Russo, S. P.; McConville, C. F.; Daeneke, T.; Kalantar-Zadeh, K. Printing two-dimensional gallium phosphate out of liquid metal. *Nat. Commun.* **2018**, *9*, 3618.

(35) Polking, M. J.; Han, M.; Yourdkhani, A.; Petkov, V.; Kisielowski, C. F.; Volkov, V. V.; Zhu, Y.; Caruntu, G.; Alivisatos, A. P.; Ramesh, R. Ferroelectric order in individual nanometrescale crystals. *Nat. Mater.* **2012**, *11*, 700-709.

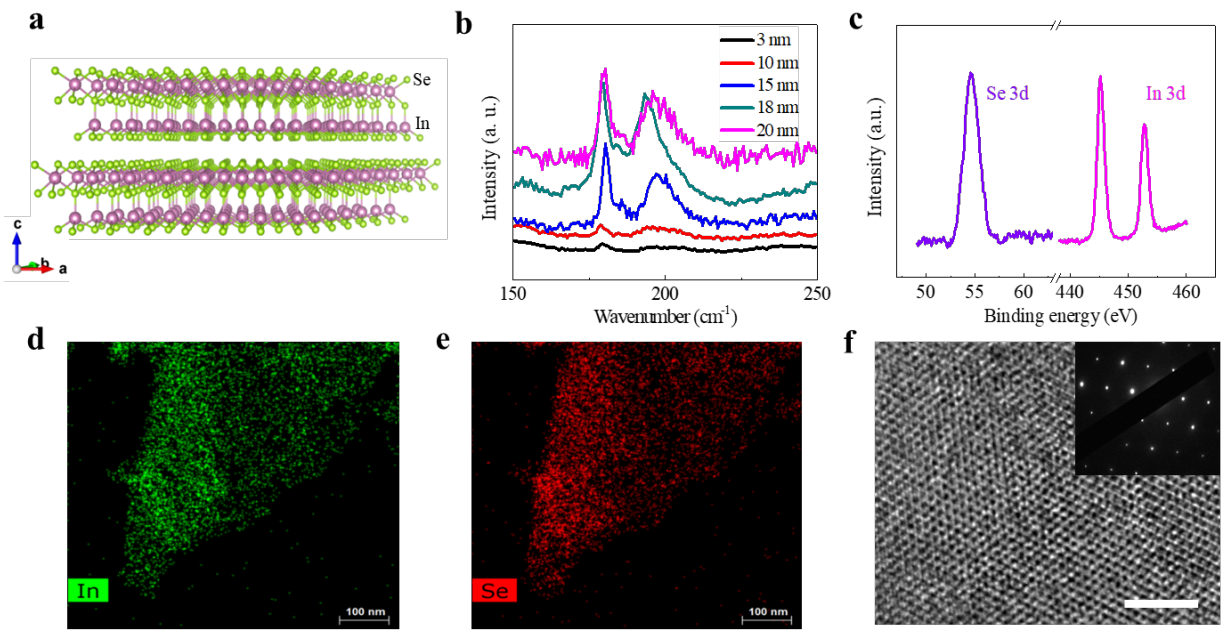

Figure 1. Structural characterizations of α-In_2Se_3. (a) Atomic structure of In_2Se_3. (b) Thickness dependent Raman spectra of In_2Se_3. (c) XPS spectra of In_2Se_3. (d-e) Elemental mapping of In and Se. (f) High-resolution TEM image of In_2Se_3 and the inset shows SAED pattern of In_2Se_3 (scale bar, 3 nm).

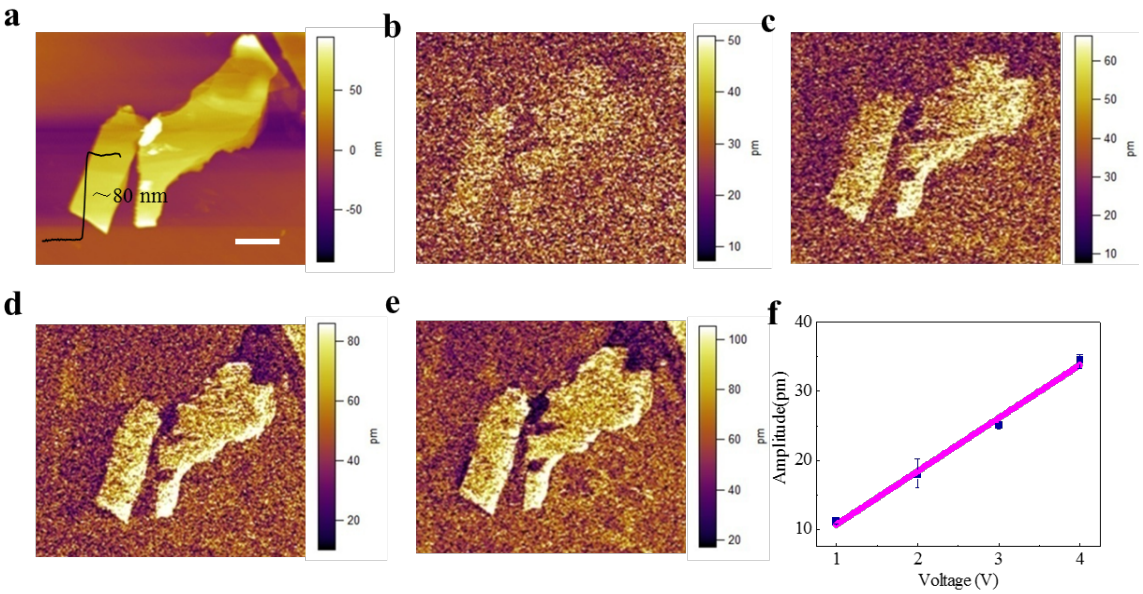

Figure 2. Amplitude images of In_2Se_3 onto SiO_2/Si substrate with different drive voltages. (a) The surface topography and height profile of In_2Se_3 exfoliated onto SiO_2/Si substrate, scale bar, 2.5 μm. (b) 1 V; (c) 2 V; (d) 3 V; (e) 4 V; (f) Piezoelectric amplitude *versus* drive voltage loop. The fitted linear line displays that the out-of-plane d_{33} is ~7.6 pm/V.

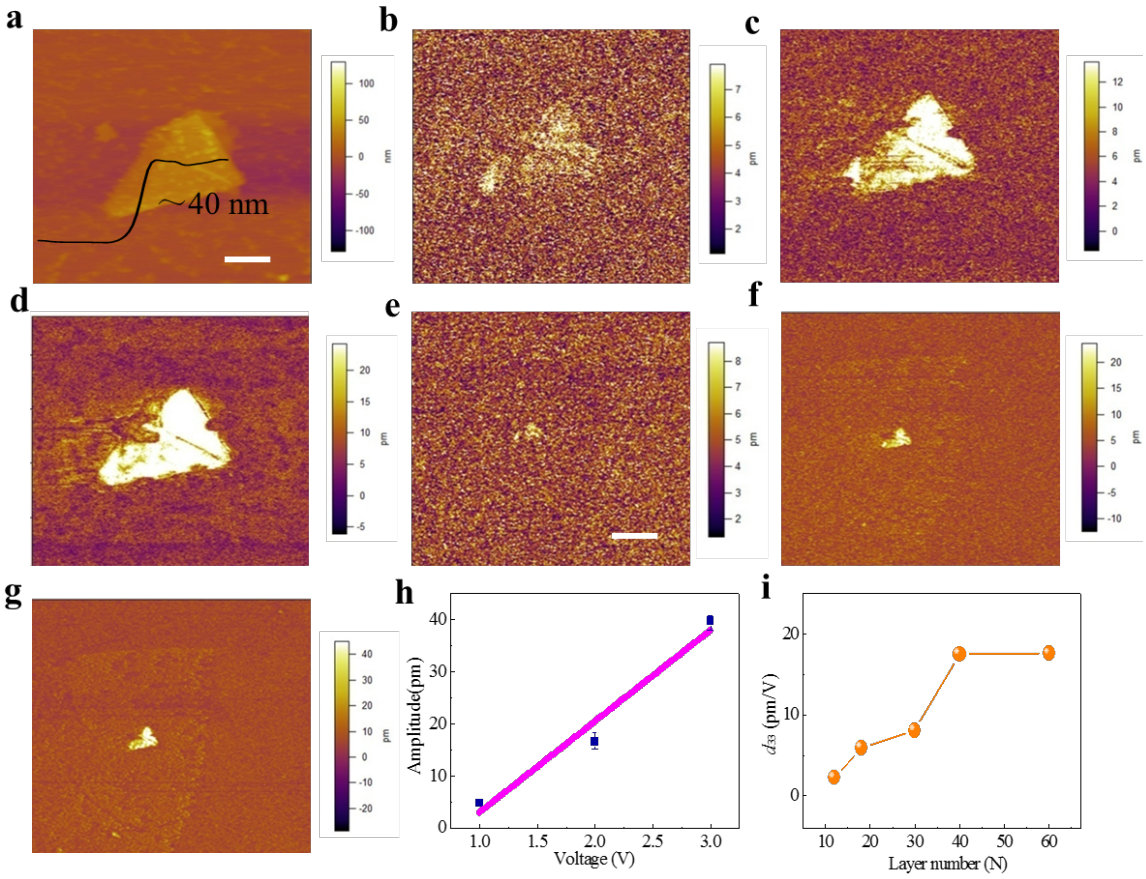

Figure 3. Piezoelectricity in In_2Se_3/MoS_2 vdW heterostructure. (a) Surface topography and the inset shows the height profile of 40 nm In_2Se_3 fabricated onto monolayer MoS_2 (scale bar, 1.5 μm). The PFM amplitude images of In_2Se_3/MoS_2. (b) 1 V; (c) 2 V; (d) 3 V. The larger scale PFM amplitude images of In_2Se_3/MoS_2 (scale bar, 5.5 μm). (e) 1 V; (f) 2V; (g) 3V, exhibiting remarkable piezoelectricity. (h) Amplitude *versus* drive voltage loop of In_2Se_3/MoS_2 heterostructure. (i) Thickness dependence of the piezoelectric coefficient d_{33} of In_2Se_3/MoS_2.

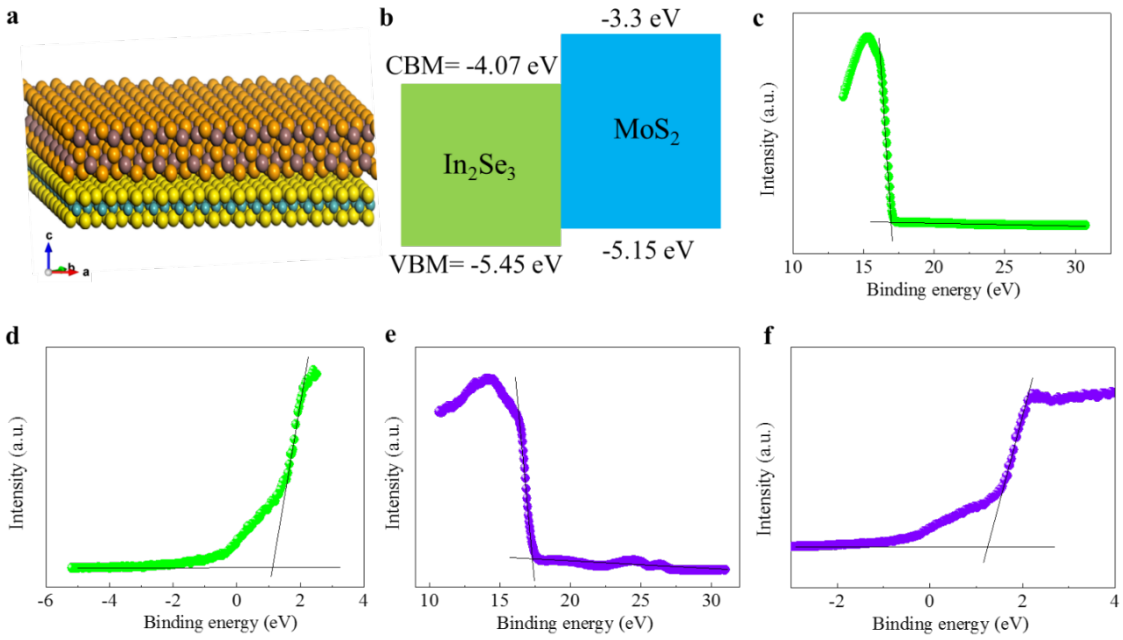

Figure 4. Energy band diagram of vdW heterostructure. (a) Atomic structure of In_2Se_3/MoS_2. (b) Schematic band structure of In_2Se_3/MoS_2. (c-d) UPS spectra of In_2Se_3. (e-f) UPS spectra of MoS_2.

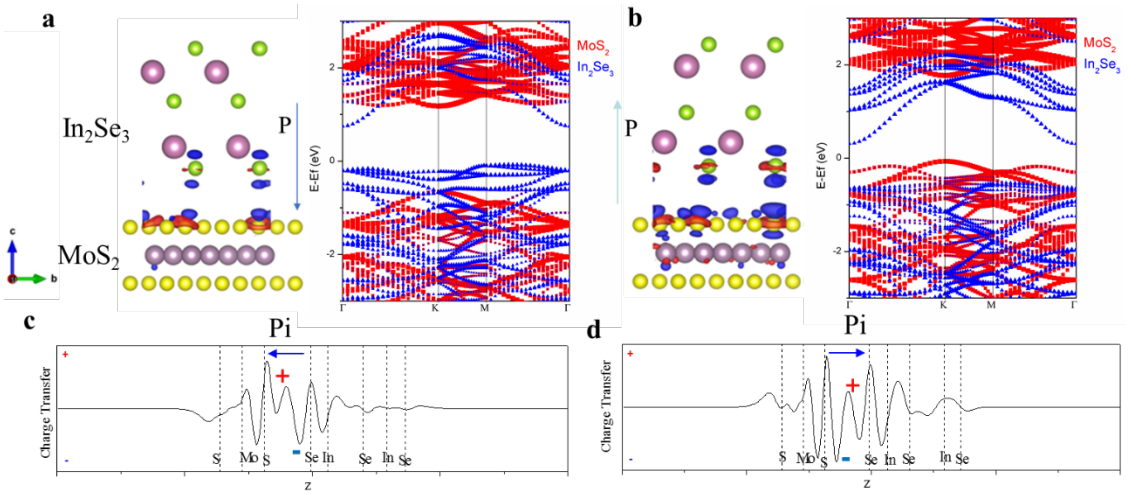

Figure 5. DFT calculations. (a) Atomic structure and band structure of the In_2Se_3/MoS_2 heterostructure when the polarization of In_2Se_3 is pointing downward. (b) The atomic structure and band structure of the In_2Se_3/MoS_2 heterostrucutre with polarization pointing upward. The charge density difference between the heterostructure and its components is plotted overlap above the atomic structure, $\Delta n = n_{In2Se3/MoS2} - n_{In2Se3} - n_{MoS2}$, the red and the blue colours denote the charge accumulation and deplection, respetviely. (c-d) is the plane-averaged differential charge density of (a-b), respetively.

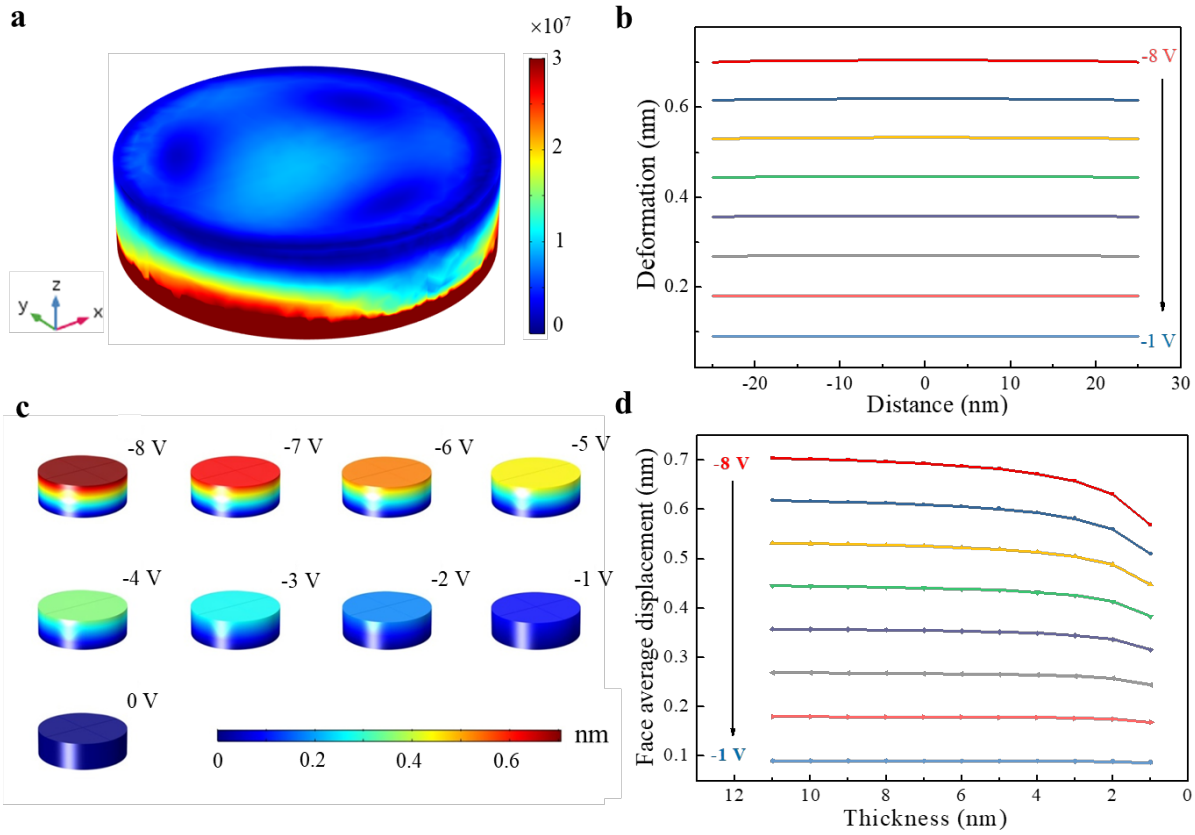

Figure 6. Simulation of the atomical deformation actuator based on out-of-plane piezoelectricity. (a) Deformation of 11 nm In_2Se_3 with an applied voltage of −8 V. (b) Deformation of upper surface of In_2Se_3 at different applied voltage. (c) Surface deformation of In_2Se_3 at different voltages. (d) The thickness dependence of surface deformation for the In_2Se_3.

TOC graphic